

DETERMINISTIC UNSTEADY VORTICITY FIELD IN A DRIVEN AXISYMMETRIC CAVITY FLOW

DANIEL RUSCH, AXEL PFAU, JOËL SCHLIENGER, ANESTIS I. KALFAS, AND REZA
S. ABHARI

Institute of Fluid Dynamics, Swiss Federal Institute of Technology
ETH Zentrum, ML H32, CH-0892 Zurich
rusch@ifd.mavt.ethz.ch

[Received: November 21, 2003]

Abstract. This paper introduces a new data visualization technique for the evaluation of 3D unsteady data using the various terms of the deterministic unsteady vorticity transport equation. The toroidal vortex residing in the inlet cavity of an axial turbine rotor labyrinth is discussed using the proposed technique. Especially, secondary flow effects and the effect of unsteadiness with respect to its contribution to loss generation were investigated. The analysis has allowed further insight in flow physics. It turned out that the rotational acceleration of the vortex shows a phase shift of one quarter of blade passing period relative to the vortex strength.

Mathematical Subject Classification: 73A05

Keywords: toroidal vortex, visualization technique, vorticity transport equation

Nomenclature

C	$[-]$	circumferential position, θ/p_{blade}
f_{bp}	$[Hz]$	blade passing frequency
h	$[J/kg]$	specific enthalpy
\vec{i}	$[-]$	unit vector
p	$[Pa]$	static pressure
p_{blade}	$[deg]$	blade pitch, $360^\circ/42$
r	$[m]$	radial position
R	$[-]$	radial height, $(r - r_{Hub})/(r_{Tip} - r_{Hub})$
s	$[J/(kgK)]$	specific entropy
t	$[s]$	time
t_{bp}	$[s]$	blade passing period, $1/f_{bp}$
T	$[K]$	temperature
\vec{v}	$[m/s]$	velocity vector
v_∞	$[m/s]$	undisturbed velocity
v_\perp	$[m/s]$	velocity component perpendicular to $\vec{\omega}$
v_\uparrow	$[m/s]$	velocity component parallel to $\vec{\omega}$
v_z	$[m/s]$	axial velocity component

z	[mm]	axial direction parallel to machine axis
$\hat{\alpha}$	[1/s ²]	rotational acceleration
θ	[deg]	angular position
ρ	[kg/m ³]	density
σ	[m]	coordinate along a vortex line
$\Delta\sigma$	[m]	coordinate increment along a vortex line
τ	[N/m ²]	stress tensor
$\vec{\omega}$	[1/s]	vorticity vector
ω_θ	[1/s]	circumferential component of $\vec{\omega}$
$\hat{\omega}$	[1/s]	rotational speed
Y	[-]	non dimensional time, t/t_{bp}

1. Introduction

One of the key issues in modern turbomachinery design is the improvement of component efficiency. The aerodynamic efficiency of a turbine stage is drastically reduced by secondary flows. Langston [1] estimates the contribution of the secondary loss to be up to 50% of the total aerodynamic loss. Hence, secondary flow control plays a key role in the strive for more efficient and environmentally friendly turbomachines. This goal can only be reached through improved understanding of the secondary flow development and interactions. There have been a number of investigations focusing on the total pressure loss coefficients, secondary velocity [2] and - in more recent papers - the vorticity distribution[3].

Pullan and Denton [4] presented a visualization method using a passive scalar technique which was found to greatly enhance the analysis of their numerical simulations of vortex-blade interaction. The kinematic behaviour of a stator passage vortex within the downstream rotor has been studied both with and without the influence of rotor endwall flows.

A large body of research work has been devoted to secondary flows within turbomachines. Sieverding [5] has summarized recent progress in the understanding of basic aspects of secondary flows in turbine blade passages and Langston [1] recently presented a comprehensive review of secondary flows in axial turbines.

Gregory-Smith et al. [6] showed a method of evaluating streamwise vorticity from traverse data and obtaining a streamwise direction from a least-squares linear fit of pitchwise averaged yaw and pitch angles. This method produces a reduced streamwise vorticity that indicates the number of rotations that a lump of fluid with such a vorticity would make as it travelled the distance between the blade rows.

Roth [7] examined existing extraction algorithms and analyzed their underlying definitions of a vortex. He proposed an elementary operation on a pair of vector fields to be used as a building block for defining and computing global line-type features of vector or scalar fields.

The present work proposes a novel technique to analyze complex flow fields involving vortical structures. Considering the terms of the vorticity equation, such as the

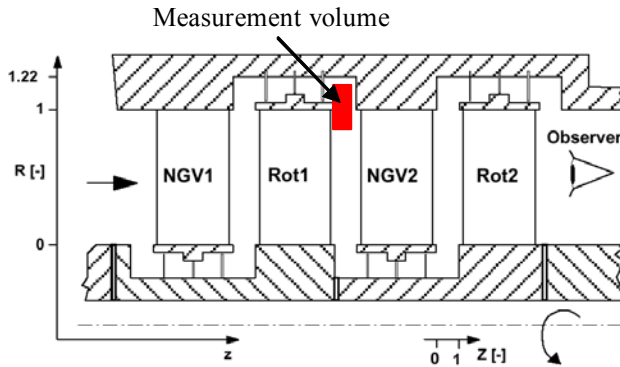


Figure 1. Geometry overview. The box indicates the location of the measurement volume

vortex stretching and the time derivative term, a deeper insight in flow physics is gained.

1.1. Experimental setup. The data presented in this paper were taken from a two-stage axial research turbine, which is described in detail in Sell et al. [8]. All measurements were taken at the same operating point using a single sensor fast response aerodynamic pressure probe (FRAP) [9,10]. The raw data is phase-lock averaged using an accurate rotor trigger and finally reduced to the requested time resolved flow parameters such as the 3D, unsteady velocity vector, as well as the total and static pressure.

The location of the measurement volume is indicated in Figure 1. The resolved volume covers both the cavity and a part of the main flow region. The coordinate system is defined as follows: C denotes the non-dimensional circumferential and R the non-dimensional radial position. According to the definition, $R = 1$ represents the tip radius. The z axis denotes the axial direction as indicated in Figure 1. A local axial coordinate axis is introduced denoting the first measurement plane with $z = 0$. The last of the 5 measurement planes is found at $z = 7.5 \text{ mm}$.

As an example, how secondary flow effects the cavity flow situation, the time averaged total pressure distribution downstream the second nozzle guide vane (NGV2) is depicted in Figure 2. The data range covers both, main and cavity flow in radial direction and 1.1 pitches in circumferential direction. The hub is located at $R = 0$ and the tip at $R = 1$, respectively. In order to visualize the periodicity of the flow, the results are copied three times in circumferential direction. The view is from a downstream position into the upstream direction. The flow region of low total pressure behind the blade shows the typical wake-loss core structure in the main flow. Both the passage vortices at the hub as well as at the tip can be clearly identified. These loss cores are created by the passage vortices, which entrain all incoming boundary layer fluid and move it to the suction side of the wake. The cavity flow regions at

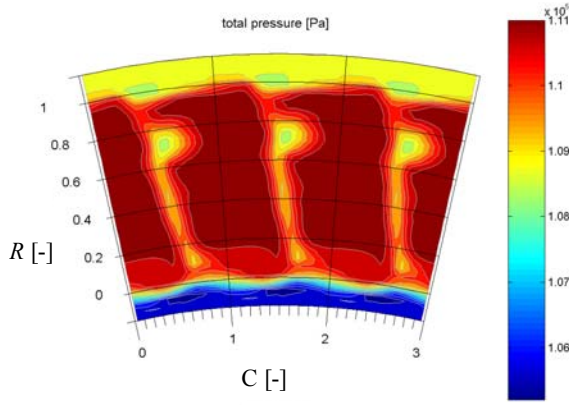


Figure 2. Total pressure distribution downstream of the second stator (NGV2)

hub and tip are characterized with significantly lower total pressure. The interface between main and cavity flow both at hub and tip shows a wavy structure.

1.2. Data Postprocessing. The new flow visualization technique bases on the vorticity transport equation Eq. (1.2). The resolution of the volume data set in both space and time is high enough to evaluate derivatives using finite differences. For each time step, the unsteady vorticity field is evaluated directly using the definition

$$\omega = \nabla \times \vec{v}. \quad (1.1)$$

Having both, the full three dimensional time resolved vorticity and velocity field, the evaluation of the substantial derivative within the compressible unsteady vorticity transport equation Eq. (2.1) [11] is straight forward using its definition Eq.(1.3).

$$\frac{D}{Dt} \left(\frac{\vec{\omega}}{\rho} \right) = \frac{1}{\rho} \vec{\omega} \cdot \nabla \vec{v} + \frac{1}{\rho^3} \nabla \rho \times \nabla p + \frac{1}{\rho} \nabla \times \left(\frac{1}{\rho} \nabla \cdot \tau \right), \quad (1.2)$$

$$\frac{D}{Dt} \left(\frac{\vec{\omega}}{\rho} \right) = \frac{\partial}{\partial t} \left(\frac{\vec{\omega}}{\rho} \right) + (\vec{v} \cdot \nabla) \left(\frac{\vec{\omega}}{\rho} \right). \quad (1.3)$$

For visualization reasons, both terms on the right hand side of Eq. (1.3) were evaluated and discussed in [12] as they allow to flip between the Lagrangian and the Eulerian point of view and describe the acceleration of the vortices. Besides the acceleration term, the new flow visualization technique bases especially on the vortex stretching term

$$\frac{1}{\rho} \vec{\omega} \cdot \nabla \vec{v}, \quad (1.4)$$

which describes the vortex tilting and stretching. A discussion of this term and its application to flow field visualization will be done in the next section.

From the application point of view, the baroclinic generation term

$$\frac{1}{\rho^3} \nabla \rho \times \nabla p \quad (1.5)$$

cannot be derived from measurements. The missing information is the unsteady temperature distribution. Together with the static pressure distribution, the time resolved density field could be evaluated. For the evaluation of the other terms in Eq.(1.2), the lack of accurate density information has only a minor influence, since the values of the temperature distribution are within a relatively narrow band.

Nevertheless, it is worthwhile to theoretically discuss the baroclinic vorticity generation term as it can be related to the entropy distribution. Taking the curl of

$$Tds = dh - \frac{1}{\rho} dp \text{ or } T\nabla s = \nabla h - \frac{1}{\rho} \nabla p \quad (1.6)$$

using $\nabla \times \nabla h \equiv 0$, Eq. (1.6) can be written as

$$\nabla \times (T\nabla s) = \nabla \times \nabla h - \nabla \times \left(\frac{1}{\rho} \nabla p \right) = -\nabla \times \left(\frac{1}{\rho} \nabla p \right). \quad (1.7)$$

Using Eq. (1.7) and the vector identity (Wilcox [13])

$$\nabla \times \left(\frac{1}{\rho} \nabla p \right) = \frac{1}{\rho} \nabla \times \nabla p + \nabla \frac{1}{\rho} \times \nabla p = \nabla \frac{1}{\rho} \times \nabla p \quad (1.8)$$

the following relation can be derived:

$$\frac{1}{\rho^3} \nabla \rho \times \nabla p = \frac{1}{\rho} \nabla T \times \nabla s. \quad (1.9)$$

In addition to the ideal gas law, Eq. (1.9) represents three coupled differential equations for the time resolved entropy. However, the time resolved temperature measurement is missing for the presented data set.

2. Results

In this section, the toroidal vortex located at the inlet cavity of a turbine rotor labyrinth seal - as discussed by Pfau et al. [14] - is under investigation applying both standard as well as the new proposed visualization technique using the vortex stretching term (1.4). The cavity vortex is driven by the main flow due to viscous interaction. The behavior of this vortex is of interest, as it affects the leakage mass flow over the shroud and redirects cooling air in cooled turbines.

2.1. Steady 3D flow visualization using total pressure. A useful property to study loss generation is the steady total pressure. The corresponding distribution downstream of the second stator is given in Figure 3. Five radial cuts and one axial cut, which is located at $z = 0$, were used to intersect the measurement volume. In addition, streamlines were added in order to visualize the flow.

From the total pressure distribution, the volume under investigation can be split into two regions, one being the main flow region ($R < 1$) which is represented by

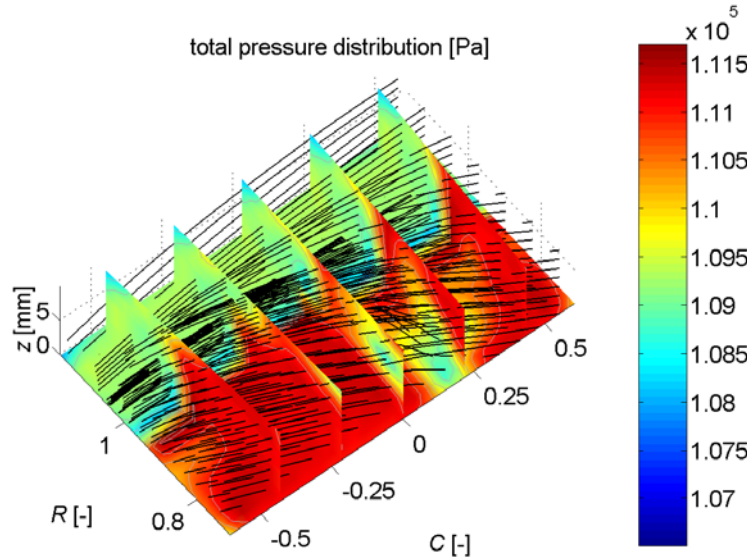


Figure 3. Total pressure distribution behind a stator visualized using radial slices. The black lines represent streamlines

high total pressure and the other being the cavity flow region ($R > 1$), which is characterized by low total pressure. The motion of the main flow shows a large circumferential component as expected downstream of swirl generating stator. The location of low total pressure within the main flow represents the loss core as found in Figure 2.

Within the cavity, the presence of the toroidal vortex aligned in circumferential direction can be verified by observing the streamlines which show very small axial motion and even back flow at the outer part. A qualitative description of the flow situation within the cavity is depicted in Figure 4. The axial component of the velocity $v_z(r)$ is constant in the main flow region and then decays while moving into the cavity. At the centre of the ring vortex, the sign changes and finally the fluid comes to rest due to the non-slip condition at the cavity wall.

2.2. Unsteady 3D flow visualization using static pressure and the circumferential vorticity component. In this section, the unsteady flow structure in the measurement volume is investigated. At first, the time resolved static pressure distribution is given in Figure 5. The different plots are equidistant in time and represent the flow during one blade passing period.

Vortices create a local minimum of static pressure in their centre of rotation. The vortex gets stronger if the static pressure in the centre is decreased. The toroidal vortex located in the cavity ($R > 1$) can be identified with this reflection in the plot

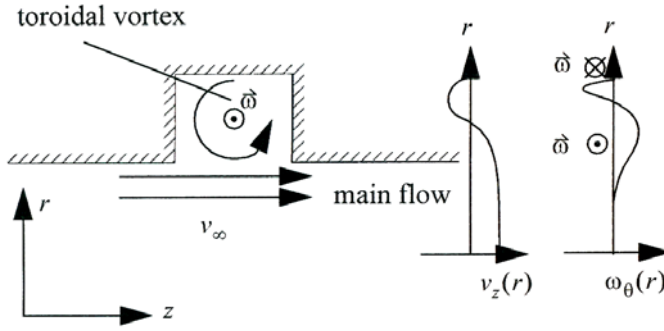


Figure 4. Generic cavity flow structure in an (r, z) cut: expected axial velocity and circumferential vorticity distribution

as a region of low static pressure. This zone of the flow is pointed out in the middle radial cut of Figure 5 using a black circle. Looking at this region for a blade passing period, it can be seen that the level of the static pressure doesn't remain constant. It shows a cyclic change where the pressure level within this middle radial cut reaches its minimum between $Y = 1/6$ and $Y = 2/6$. The cyclic change is correlated to the blade passing period.

Figure 6 shows the circumferential component of the vorticity vector ω_θ . Considering the cavity flow model depicted in Figure 4, it can be stated that ω_θ changes while going radially outward through the cavity: As ω_θ is proportional to the slope of the axial velocity v_z , it vanishes in the main flow region, where v_z is about constant. In the tip zone, v_z decays and therefore ω_θ gets positive and stays positive as long as the slope of the axial velocity profile shows the same sign. At maximum negative axial velocity, ω_θ is zero. At this radial position, ω_θ changes its sign and remains negative until the cavity wall is reached. The presented idealized radial distribution of the circumferential component of the vorticity vector can also be found in the unsteady measurements presented in Figure 6, considering one of the radial cuts. ω_θ vanishes in the undisturbed main flow. Going radially outward, ω_θ shows at first positive and then negative values as discussed. Moreover, the transient behavior is as expected from the previous reflections on the static pressure distribution. Looking again at the middle radial cut, a maximum value is reached between $Y = 1/6$ and $Y = 2/6$.

A monitor point was selected at the middle radial slice within the core of the cavity vortex as indicated in Figure 5 with the black dot. The behavior of p and ω_θ at this point during 3 blade passing periods is given in Figure 8 and allows a direct transient comparison between p and ω_θ . It is evident that ω_θ increases by as much as 100% in a negative pressure gradient zone and decreases gradually by as much in a positive pressure gradient area. Clearly and as expected, the circumferential vorticity and the gradient of the static pressure in the cavity are inversely related.

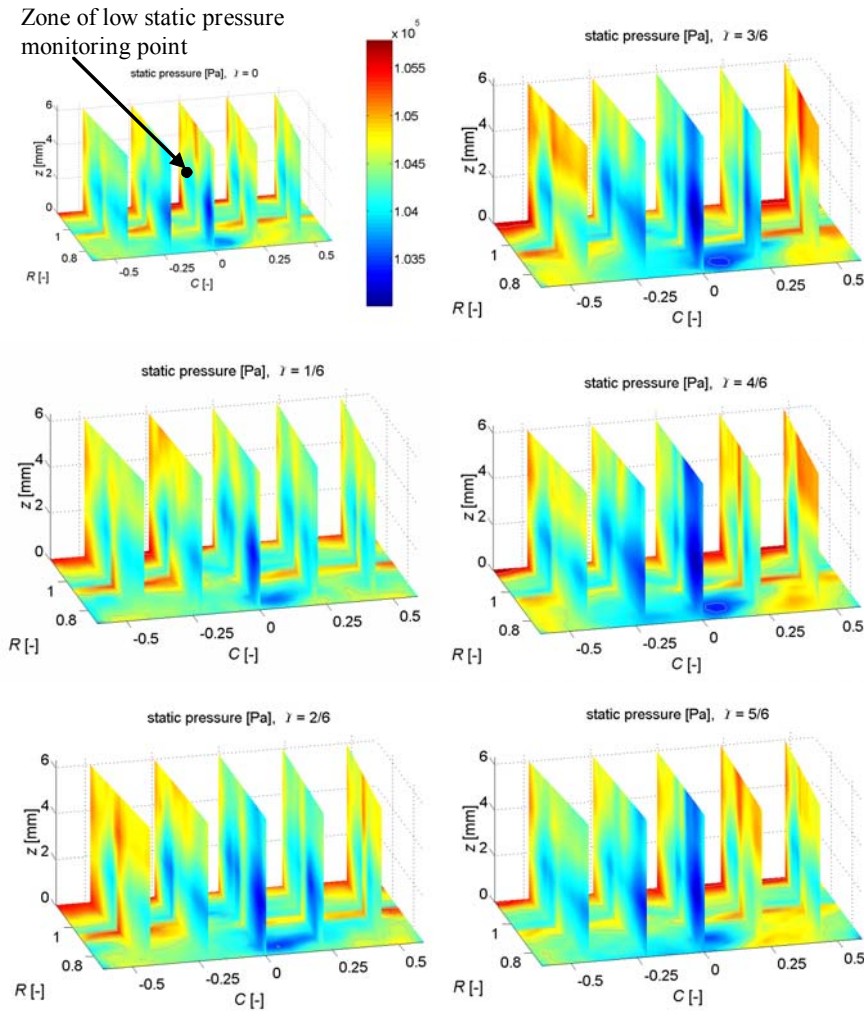


Figure 5. Unsteady static pressure distribution downstream of the second stator: One blade passing period

2.3. Unsteady 3D flow visualization using the circumferential component of the vortex stretching term. In Figure 7, the circumferential component of the vortex stretching term is depicted. Consider a vortex line in a velocity field as indicated in Figure 9. According to the definition, vortex lines are tangential to the local vorticity vector $\vec{\omega}$. The local velocity vector \vec{v} can be split into a component tangential v_{\parallel} and a component normal v_{\perp} to the vortex line as it is described in [15].

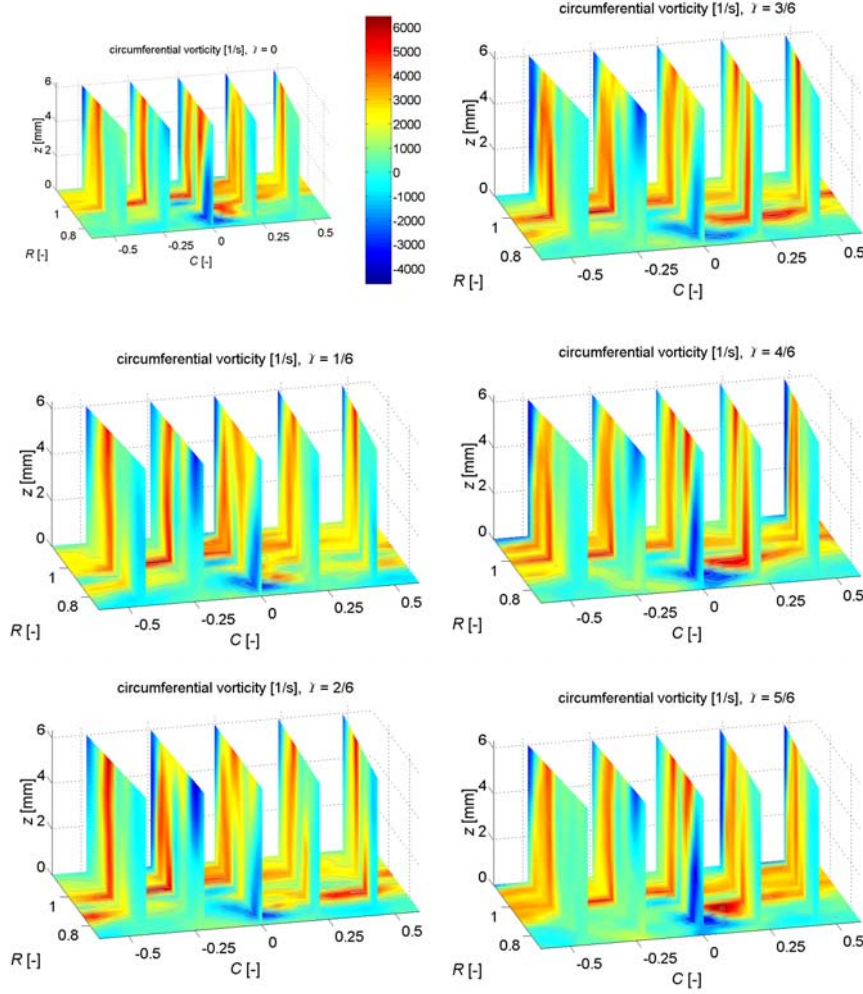


Figure 6. Unsteady circumferential vorticity component downstream of the second stator: One blade passing period

Neglecting the density, term (1.4) can be written as

$$\vec{\omega} \cdot \nabla \vec{v} = \left[\vec{\omega} \cdot \left(\vec{i}_\sigma \frac{\partial}{\partial \sigma} + \vec{i}_n \frac{\partial}{\partial n} + \vec{i}_m \frac{\partial}{\partial m} \right) \right] \vec{v} = |\vec{\omega}| \frac{\partial}{\partial \sigma} \vec{v} = |\vec{\omega}| \frac{\partial}{\partial \sigma} \vec{v}_\uparrow + |\vec{\omega}| \frac{\partial}{\partial \sigma} \vec{v}_\perp, \quad (2.1)$$

where σ denotes the coordinate along the vortex line, n away from the center of curvature and m along the third normal. Eq. (2.1) makes use of $\vec{\omega} \cdot \vec{i}_n = \vec{\omega} \cdot \vec{i}_m = 0$ and $\vec{\omega} \cdot \vec{i}_\sigma = |\omega|$. Considering the derivative of the first term in Eq. (2.1) to be positive, which corresponds to the case that $\vec{v}_\uparrow(\sigma + \Delta\sigma) > \vec{v}_\uparrow(\sigma)$, the section of

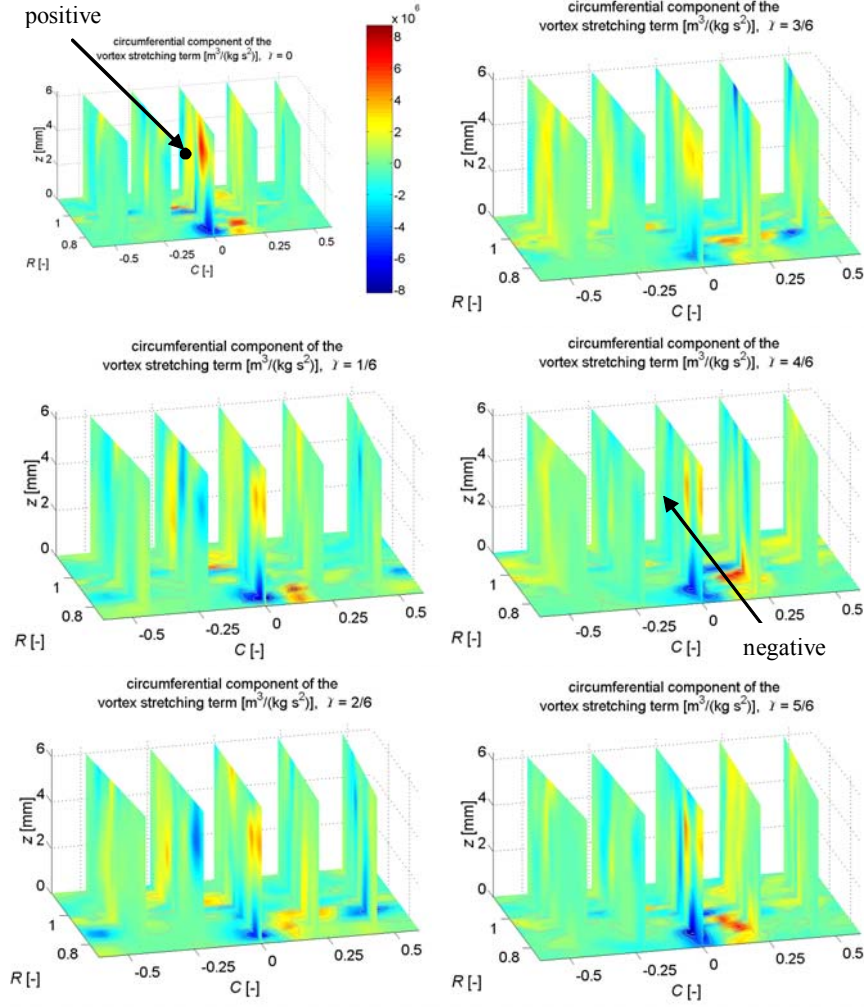


Figure 7. Unsteady component of the circumferential vortex stretching term downstream of the second stator: one blade passing period

the vortex tube under observation will be stretched and the rotational speed will increase as the tube diameter decreases (see Figure 9). The opposite behavior is true for $\vec{v}_{\uparrow}(\sigma + \Delta\sigma) < \vec{v}_{\uparrow}(\sigma)$. The second term on the right hand side of Eq. (2.1) is responsible for the vortex tilting as can be seen by considering $\vec{v}_{\perp}(\sigma + \Delta\sigma) \neq \vec{v}_{\perp}(\sigma)$. Going back to Figure 7, one can see that the circumferential component of the vortex stretching term undergoes a cyclic change as well. At $Y = 0$ the stretching term is positive, whereas it is negative at $Y = 3/6$, looking again at the middle radial cut. As mentioned before, a positive component in the direction of the vortex line represents

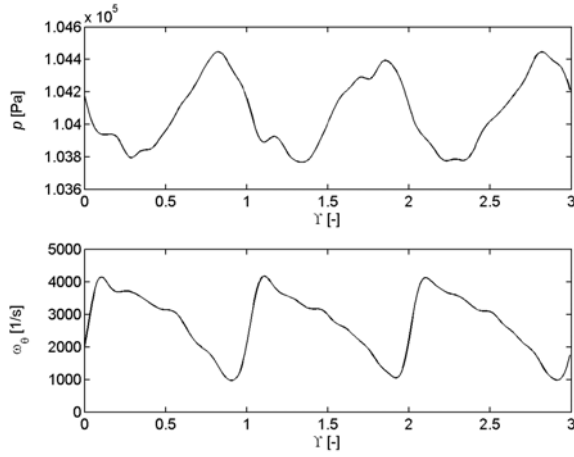


Figure 8. Time series of static pressure and circumferential vorticity component

a stretching of the vortex and a negative one squeezes the vortex, if the vortex is aligned with the stretching term vector. In case of the toroidal vortex, the vortex is aligned in circumferential direction and the vortex stretching term will therefore primarily stretch (rather than tilt) the vortex and thus increase the strength of the circumferential vorticity component and decrease the static pressure in its core. The opposite is true for the negative vortex stretching term, which is consistent with the findings up to now. It has to be stated, that the vortex stretching term is ahead of the vortex strength term. That means that the vortex stretching term reaches its maximum before the vortex strength term does. Therefore, the spin up process of the vortex needs some time, which is discussed in the following paragraph.

At $Y = 3/6$, the vortex stretching term in circumferential direction is negative and thus squeezes the vortex. As it can be seen in Figure 5, the strength of the vortex will decrease. The behaviour found in the experiment can be explained by considering a solid body rotation. Let $\hat{\omega}$ denote the rotational speed of the vortex expressed as a harmonic function according to $\hat{\omega} = \bar{\omega} + \omega' \sin(\omega_{bp}t)$ with $\omega_{bp} = 2\pi f_{bp}$. The rotational acceleration is then the time derivative of the rotational speed $\hat{\alpha} = \frac{\partial}{\partial t} \hat{\omega} = \omega_{bp} \omega' \cos(\omega_{bp}t)$ and is thus a quarter of a period ahead of the rotational speed. This is exactly the behaviour found in the measurements: The acceleration term represented by the circumferential component of the vortex stretching is a quarter of a period ahead of the terms which represent the speed or the strength of the vortex (such as the static pressure distribution and the circumferential component of the vorticity).

3. Conclusions

Nowadays, sophisticated probe technology and high computational power make it possible to analyze complex flow in four dimensions, i.e. space and time. Considering

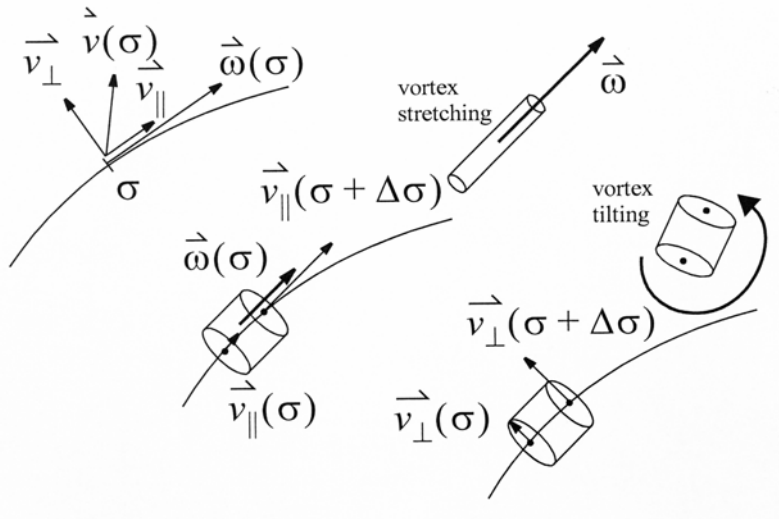


Figure 9. Influence of the velocity field on the vorticity

the huge amount of data, intuitive visualization is the key for further processing and analyzing data as well as to locate interesting features. It allows to gain insight in physical mechanisms and promotes flow understanding.

The visualization of the vortex stretching term of the deterministic unsteady vorticity transport equation has proven to be a powerful tool. It makes it possible to locate complex features in the flow, such as the toroidal vortex and to associate different properties with each other. In the example under investigation, the stretching and squeezing of the vortex line around the annulus could be connected with the transient behavior of the static pressure and the circumferential component of the vorticity vector distribution.

The baroclinic vorticity generation term was related to the gradient of the entropy. For the evaluation of the entropy differences, the temperature distribution has to be time resolved. Hence, the time resolved temperature measurement is a very important research area for the future as it would allow to calculate entropy differences.

Acknowledgement. The flow measurements in the turbine were supported by the German Federal Ministry of Economy (BMWI) under file numbers 0327060D and 0327060F. The authors gratefully acknowledge AG Turbo, Alstom Power and Rolls-Royce Germany for their support and permission to publish this paper.

REFERENCES

1. LANGSTON, L.S.: Secondary flows in axial turbines - a review. *Anal. of the New York Academy of Sciences*, **934**, (2001), 11-26.

2. CHALUVADI, V.S.P., KALFAS, A., HODSON, H.P., OHYAMA, H. AND WATANABE, E.: *Blade row interaction in a high pressure steam turbine*. Journal of Turbomachinery, **125**, (2003), 14-25.
3. TREIBER, M., ABHARI, R.S. AND SELL, M.: *Flow physics and vortex evolution in annular turbine cascades*, ASME Turbo Expo 2002, GT-2002-30540.
4. PULLAN, G. AND DENTON, J. D.: Numerical simulation of vortex turbine blade interaction, paper NO TA-106, *Proceedings of the 5th European Turbomachinery Conference*, Prague, Czech Republic, March 17-22, (2003), 1049-1059.
5. SIEVERDING, C.H.: Recent Progress in the Understanding of basic aspects of secondary flows in turbine blade passages. *ASME J. Eng. for Power*, 107(2), (1985), 248-257.
6. GREGORY-SMITH, D.G., GRAVES, C.P. AND WALSH, J.A.: Growth of secondary losses and vorticity in an axial turbine cascade. *ASME J. Turb.*, 110, (1988), 1-8.
7. ROTH, M.: *Automatic Extraction of Vortex Core Lines and Other Line-Type Features for Scientific Visualization, Selected Readings in Vision and Graphics*, Volume 9, Hartung-Gorre Verlag, Kostanz, ISSN 1439 - 5053, ISBN 3-89649-582-8, (2000).
8. SELL, M., SCHLIENGER, J., PFAU, A., TREIBER, M., AND ABHARI, R.S.: The 2-stage axial turbine test facility LISA, *Proceedings of the ASME Turbo Expo, 2001-GT-492*, June 4-7, New Orleans, Louisiana.
9. PFAU, A., SCHLIENGER, J., KALFAS, A.I. AND ABHARI, R.S.: Unsteady, 3-dimensional flow measurement using a miniature virtual 4 sensor Fast Response Aerodynamic Probe (FRAP), GT2003-38128, *ASME Turbo Expo*, 16-19 June 2003, Atlanta.
10. SCHLIENGER, J., PFAU, A., KALFAS, A.I. AND ABHARI, R.S.: Effects of labyrinth seal variation on multistage axial turbine flow, *Proceedings of ASME Turbo Expo*, GT-2003-38270, 16-19 June 2003, WCC, Atlanta, Georgia, USA.
11. THOMPSON, P.A.: *Compressible Fluid Dynamics*, McGraw-Hill, New York, (1972).
12. RUSCH, D.: *Evaluation of the Steady and Unsteady Vorticity Field from Experimental Data*, Semester Thesis, Turbomachinery Laboratory, ETH Zurich, 2002.
13. WILCOX, D.C.: *Basic Fluid Mechanics*, DCW Industries, Inc., California, 1997.
14. PFAU, A., SCHLIENGER, J., RUSCH, D., KALFAS, A.I. AND ABHARI, R.S.: Unsteady Flow Interactions within the Inlet Cavity of a Turbine Rotor Tip Labyrinth Seal, GT2003-38271, *ASME Turbo Expo*, 16-19 June 2003, Atlanta.
15. KUNDU, P.K. AND COHEN, I.M.: *Fluid Mechanics*, Second Edition, Academic Press, New York, 2002, 139-140.